c-Axis Conductivity and Intrinsic Josephson Effects in $YBa_2Cu_3O_{7-\delta}$

M. Rapp, A. Murk, R. Semerad, and W. Prusseit
Physik Department E10, Technische Universität München, 85747 Garching, Germany
(Received 3 April 1996)

We have observed intrinsic Josephson coupling between CuO_2 double layers of $YBa_2Cu_3O_{7-\delta}$ by direct detection of ac and dc Josephson effects. The crucial points were a reduction of the junction size to the $1-2$ μm range and a weakening of the interlayer coupling via oxygen depletion of the CuO chains. As a result we obtained distinct signatures in the *I-V* characteristics and 11 GHz microwave emission caused by ac Josephson currents. The temperature dependence of the critical current supports the idea of a superconductor-insulator-superconductor interlayer tunneling mechanism. [S0031-9007(96)00808-3]

PACS numbers: 74.50.+r, 74.60.Jg, 74.72.Bk, 74.80.Dm

The layered structure and strong anisotropy of high temperature superconductors (HTS) suggest a concept of stacked two-dimensional superconducting planes which are only weakly coupled in the *c* direction by Josephson effects (JE). This viewing of the superconductor as a sequence of intrinsic Josephson junctions has found its striking confirmation in the experiments by R. Kleiner *et al.* on $Bi_2Sr_2CaCu_2O_8$ (BSCCO) and $Tl_2Ba_2Ca_2Cu_3O_{10}$ (TBCCO) single crystals [1,2]. These experiments have unambiguously revealed the SIS (superconductor-insulator-superconductor) tunneling character of the *c*-axis transport current in highly anisotropic superconductors.

However, a necessary condition for the occurrence of weak link behavior is that the order parameter is sufficiently suppressed within the barrier. This condition is perfectly met in the Bi- and Tl-based compounds where wide oxide building blocks separate the CuO_2 double or triple layers. As a direct consequence these materials exhibit an extreme anisotropy ratio $\gamma = \lambda_c/\lambda_{ab} \approx 10^2-10^3$ and the calculated effective coherence length is considerably smaller than the interlayer spacing [3].

In contrast, $YBa_2Cu_3O_{7-\delta}$ (YBCO) exhibits conductive CuO chains located right in the middle of the structure which separates the superconducting double layers. These chains may even become also superconducting by proximity effect, and it is not clear whether weak link behavior can arise at all. In completely oxygenated YBCO the chains are very effective in mediating the interlayer charge transfer which finds its expression in the low anisotropy ratio of $\gamma \approx 5$. However, this mechanism should depend strongly on the concentration of chain oxygen vacancies. In fact, from a fluctuation analysis of the specific heat and in-plane conductivity the effective coherence length has been shown to drop drastically from $\xi_c = 3$ Å ($\delta = 0$) to $\xi_c = 1.4$ Å even for a slight depletion of $\delta = 0.1$ [4]. Although a mean field coherence length of this dimension has no real physical meaning, it gives a rough impression of the effective coupling strength. Correspondingly, the *c*-axis normal conductivity is expected to change its character from metallic to semiconducting [5]. Under these circumstances it should be possible to reduce or tune the interlayer coupling via oxygen content in such a way that intrinsic JE are likely to be observable.

Recently, Ling *et al.* claimed to have found evidence for intra- as well as inter-unit-cell Josephson coupling in YBCO close to the transition [6]. Modulations of the dynamic resistance versus magnetic field have been assigned to two junction widths. The smaller width of 3.5 Å, deduced from just two peaks that are not even periodic, was believed to arise from an intra-unit-cell junction between neighboring CuO_2 planes. A second length of 21 Å which has no intrinsic explanation has been calculated from a periodic pattern that, however, lacks the characteristic Fraunhofer signature, i.e., central structure twice as wide as the side maxima. Rather, it is best explained in terms of an interference pattern of two or more weak links within the crystal. In fact, the authors report that only a small fraction of the total crystal contributes to the signal. Deviations from the ideal behavior are accounted to crystal imperfections and other phases. Hence, it seems very controversial whether the observed effects are of intrinsic nature.

A series of characteristic features allows the definite proof that *c*-axis supercurrents are limited by JE: (1) In the resistive state the *I-V* characteristics should exhibit a concave curvature in contrast to a convex flux flow behavior. (2) The shape of the *I-V* curve described by a RSJ-like (resistively shunted junction) model is determined by the McCumber parameter $\beta_c = (2\pi/\Phi_0)CR_N^2I_c$, where I_c, R_N, and C are the critical current, normal state resistance, and junction capacitance, respectively. If $\beta_c > 1$, switching of single junctions leads to distinct hysteretic voltage steps where I_cR_N is in the order of the gap energy, i.e., in the mV range. In BSCCO $\beta_c \gg 1$ and the strong hysteresis of the intrinsic series array results in brushlike *I-V* characteristics with a great many of branches each corresponding to a certain number of junctions in the resistive state [1,2]. Taking typical YBCO parameters $\varrho_c = 100$ mΩ cm, $j_c = 10^6$ A/cm^2, and an estimated $\epsilon_r \approx 10$ the above expression yields $\beta_c \approx 2$. Consequently, in YBCO hysteresis is expected to be small

 0031-9007/96/77(5)/928(4)$10.00

if it shows up at all. (3) From the temperature dependence of the critical current it is possible to specify the type of Josephson coupling and to distinguish between SNS (superconductor-normal metal-superconductor) proximity or SIS-tunneling behavior. (4) If the critical current is exceeded and a finite voltage drops across the junctions, the ac Josephson effect will be detectable as a microwave emission signal where the frequency f is directly related to the voltage V via

$$f = \frac{2e}{h}\frac{V}{N} = (483.6\ \mathrm{MHz}/\mu\mathrm{V})\frac{V}{N}. \qquad (1)$$

This implies a voltage drop of 1–2 mV for a stack of $N = 50$–100 junctions radiating at a fixed detection frequency of 11 GHz.

However, in order to observe these signatures the junctions have to be small enough. For circular geometry the crossover to the long junction regime occurs for diameters around $(4 - 10)\lambda_j$ [7]. Here, the Josephson penetration depth λ_j is equivalent to the magnetic penetration depth λ_c of the material with screening currents in the c direction [2] which is in the order of 1 μm for YBCO. Because of the high critical current densities in long junctions, moving vortices will cause considerable dissipation, lead to spurious radiation, or, on the contrary, may even suppress radiation at all. Additionally, with increasing junction area it gets harder to carry off the dissipated power and self-heating becomes a problem.

The limitation of the junction size to a micron scale rules out the use of single crystals since handling is no longer practicable. Instead, we used very smooth epitaxial, c-axis oriented films and a photolithographic planar technology to realize intrinsic Josephson junctions. Batches of at least 4–7 identical YBCO films were simultaneously deposited at 670 °C on CeO_2-buffered sapphire substrates by an intermittent thermal coevaporation scheme described in detail in Ref. [8]. After cooling to room temperature in 200 mbar of dry oxygen the chamber was pumped down again, and a 30 nm thick gold contact layer was evaporated without breaking the vacuum. This procedure ensures very low contact resistivities around $10^{-8}\ \Omega\,\mathrm{cm}^2$ which are essential for a three point probe of tiny contact areas.

To remove oxygen in a well-defined way and for a direct comparison samples of each batch were annealed at 350 °C for 6 h under various oxygen pressures (10^{-1}–10^{-3} mbar). The approximate oxygen depletion has been deduced from the established T_c variation with oxygen content as determined in a previous study [9].

The c-axis conduction geometry was realized by a standard photolithographic three layer process. Starting from the gold covered YBCO films, mesa structures of 1–2 μm diameter were defined by photoresist. Subsequently, the surrounding 350 nm thick film was milled down to 290–250 nm by 300 eV argon ions resulting in mesas of 60–100 nm height corresponding to a stack of 50–85 junctions. Immediately after ion milling a $LaAlO_3$ insulating layer was *in situ* sputter deposited to planarize the film surface. As a secondary advantage the embedding protects the sensitive mesa edges against degradation by ambient moisture, etc. The top of the mesa was laid open by lifting off the photoresist. In a final step a gold wiring layer was sputtered and patterned to provide the top contact leads to the mesa. The residual YBCO film underneath the mesa serves as superconducting counterelectrode. The remaining thickness of the bottom film has been chosen large enough so that the critical current is first exceeded in the mesa and not by the spreading currents.

To guarantee a homogeneous feed current flow and to avoid distributing currents within the mesa the top electrode has not been split into separate current and voltage leads. As mentioned above, a low contact resistance is essential in this arrangement.

The samples, which contain 18 mesas on a chip, are dc connected to a low noise current-voltage source and mounted in a chip carrier on a copper block close to an X-band waveguide (WR75). The tip of a wire through the waveguide is placed on the contact leads to couple the microwave emission signal into the waveguide which is connected to a commercial low noise 11 GHz satellite receiver. The dc voltage drop was measured by the 3-point compensation technique. In all the figures with the exception of Fig. 5 the Ohmic contact resistance has been subtracted.

Figure 1 shows the c-axis resistivity as a function of temperature for four samples annealed under different conditions with transition temperatures indicated at the curves. The assigned anisotropy ratios γ have been deduced from the resistivity ratios in ab and c directions $\gamma = \sqrt{\varrho_c/\varrho_{ab}}$ directly above the transition. Obviously, with decreasing oxygen content the c-axis transport changes from a metallic to a semiconducting behavior. Close to the metal-insulator transition the anisotropy increases drastically and we obtain γ values up to 80 for $\delta \approx 0.5$. But even a

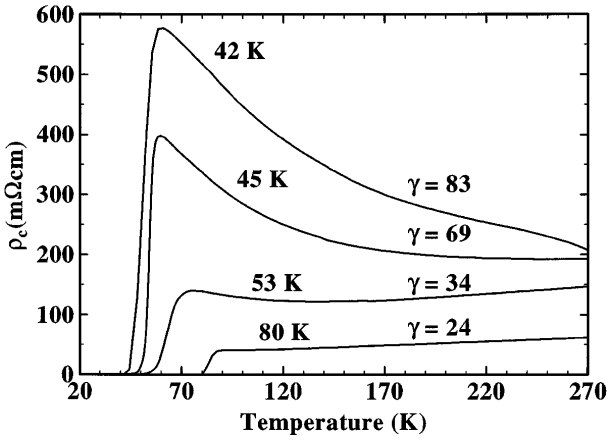

FIG. 1. Temperature dependence of the c-axis resistivity for four oxygen-depleted $YBa_2Cu_3O_{7-\delta}$ mesas with transition temperatures and anisotropy ratios as indicated.

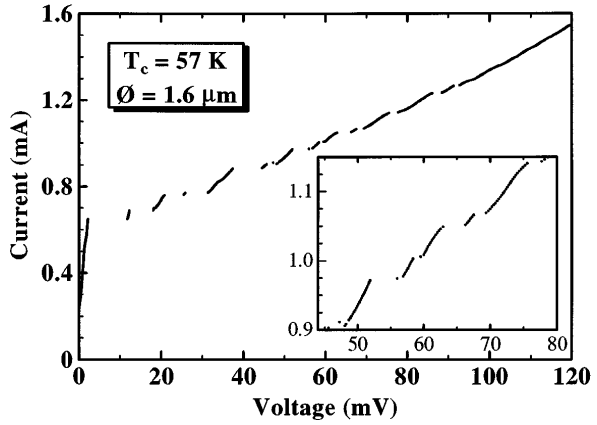

FIG. 2. Current-voltage characteristic of oxygen deficient $YBa_2Cu_3O_{7-\delta}$ ($T_c = 57$ K) recorded at 4.2 K. The inset which gives a magnified detail demonstrates a minimum I_cR_N of 1–2 mV.

moderate oxygen depletion ($\delta = 0.1-0.2$) where T_c is still above 80 K yields a considerably larger anisotropy of $\gamma \approx 20$ than found for completely oxygenated YBCO ($\gamma = 5$).

The most prominent structures in the I-V characteristics are observed in strongly depleted YBCO ($T_c \approx 50-60$ K, $\delta = 0.4-0.5$). This is demonstrated in Fig. 2 for a 1.6 μm mesa at 4.2 K. The critical currents of the individual junctions are not uniform in this case and switching of one or several junctions leads to voltage steps with a small hysteresis so that the overall curve is reminiscent of the I-V brush of BSCCO [1]. The curvature clearly rules out any flux flow behavior. The smallest jumps which may be assigned to single junctions exhibit a width of 1–2 mV (cf. inset of Fig. 2). A similar stepped characteristic for a different device is shown in Fig. 3 together with the simultaneously recorded microwave emission signal. A number of peaks is observed which arise whenever the voltage drop across a certain group of junctions within the mesa fulfills relation (1). Switching into the resistive state results in an immediate breakdown of the signal until another group of superconducting junctions is biased in such a way that the emission falls within the bandwidth of the detector again. Hence, the emission peaks are directly correlated to the voltage steps. Typically, at 4.2 K the critical current density of such depleted material lies in the range of $(5-10) \times 10^4$ A/cm^2. It should be mentioned that by changing the current path to the mesa any spurious effects which might arise from grain boundaries in the YBCO bottom electrode could be definitely ruled out.

With increasing interlayer coupling, i.e., enhanced oxygen content, β_c becomes smaller, and we cannot expect pronounced features in the I-V curves. However, the ac Josephson effect should remain untouched. The typical appearance of moderately depleted YBCO ($\delta = 0.2-0.3$) at 4.2 K is depicted in Fig. 4. The most prominent structure in the I-V curve is the 200 mV jump at 30 mA bias which corresponds to a current density of $j_c(4.2\text{ K}) = 1.5 \times 10^6$ A/cm^2. However, at this power level, the switching is mainly caused by self-heating and exhibits a large thermal hysteresis (not shown) when the current is ramped down. The important effects occur below this step, when the voltage drop across the mesa is in the range of a few millivolts. In this case, there are two broad emission peaks corresponding to two groups of junctions radiating at different biases. The inset shows the same structure plotted versus voltage in the range below the jump. For the first peak the voltage drop of 0.6 mV can be assigned to the group with the lower j_c. From Eq. (1) we estimate a number of about 25 junctions contributing to the observed peak which is consistent with the prepared total mesa height of 50 unit cells.

All data shown so far were taken at 4.2 K. With increasing temperature the I-V characteristics get rounded until jumps are smeared out. Nonetheless, microwave emission as a fingerprint of ac Josephson currents could

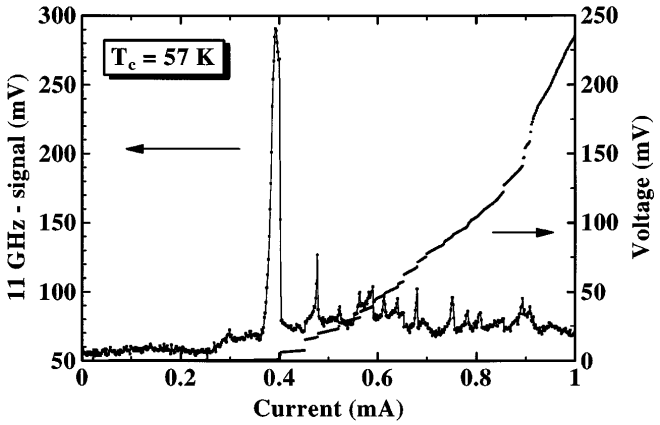

FIG. 3. Voltage vs current and related microwave emission at 11 GHz for highly oxygen deficient $YBa_2Cu_3O_{7-\delta}$ ($T_c = 57$ K) taken at 4.2 K.

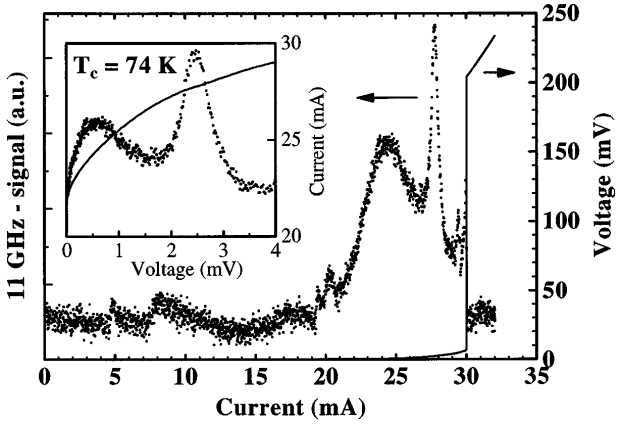

FIG. 4. Voltage vs current and 11 GHz emission for moderately depleted $YBa_2Cu_3O_{7-\delta}$ ($\delta = 0.3$) at 4.2 K. The inset shows the current and the emission signal plotted vs voltage to demonstrate the consistency with relation (1).

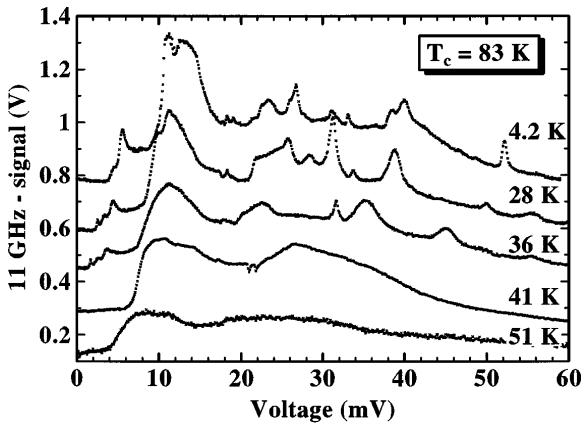

FIG. 5. Microwave emission at 11 GHz as a function of temperature. For clarity the curves are vertically shifted with respect to each other. Since the contact resistance is not purely linear, it has not been subtracted.

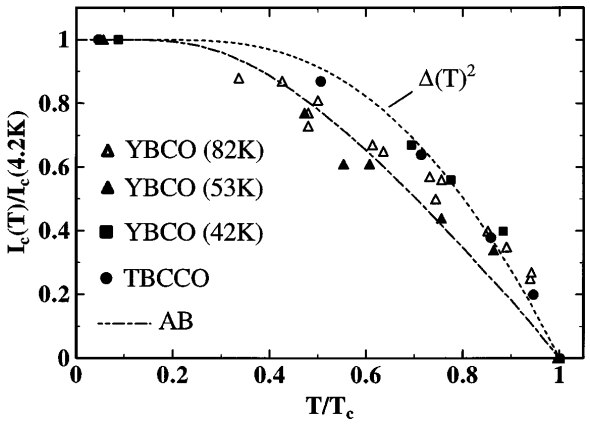

FIG. 6. Temperature dependence of the critical current in the c direction for $YBa_2Cu_3O_{7-\delta}$ films with different oxygen contents and a TBCCO sample. The transition temperatures are indicated in parentheses. Details concerning the theoretical Ambegaokar-Baratoff fit (AB) and the Δ^2 dependence are given in the text.

be detected closely up to the transition temperature. The evolution of the emission signal with temperature is shown in Fig. 5 for a slightly oxygen deficient film ($T_c = 83$ K, $\delta \approx 0.2$).

For completely oxidized YBCO ($T_c > 87$ K) we never found evidence for intrinsic JE. The dc characteristics were determined by flux flow and a purely thermal voltage jump which often led to destruction of the device. Correspondingly, besides a weak increase of the thermal noise, no microwave signal could be detected. The same holds for devices larger than 5 μm even if the films were oxygen depleted confirming the considerations above.

To elucidate the interlayer coupling mechanism in oxygen deficient YBCO and to discriminate between SIS-tunneling and SNS-proximity behavior the temperature dependence of the critical current has been evaluated for a large number of different samples. The critical current values were determined by following the evolution of characteristic features (e.g., steps) in the I-V curves or the bias currents corresponding to microwave emission peaks with temperature. Both procedures gave identical results which are depicted in Fig. 6. Data of YBCO films with various oxygen depletion are compared to theoretical models and to a TBCCO film sample patterned in the same way as described above [10]. The first theoretical fit is the Ambegaokar-Baratoff relation for classical SIS tunneling [11]. The second curve $I_c(T) \propto \Delta(T)^2$ has been suggested by Abrikosov based on the assumption of resonant interlayer tunneling through localized centers in the chains [5]. As input parameter we used the BCS gap function $\Delta(T)$ [12], and in the first case $\Delta_0/k_B T_c = 1.2$ gave the best fit to the data. Although the oxygen depletion varies considerably, in any case YBCO strongly resembles TBCCO. The overall curvature and the saturation at low temperatures is clearly in favor of SIS tunneling.

In summary, intrinsic JE have been unambiguously demonstrated in YBCO films for the first time and in the whole temperature range below T_c. The chain occupation plays a crucial role for the interlayer coupling. YBCO with completely filled chains does not show any Josephson signature, at least for a junction size $\geq 1-2$ μm. A slight depletion results in a drastic weakening of the coupling strength so that pronounced Josephson tunneling behavior can arise.

We would like to express our thanks to H. Kinder for the kind support and stimulating discussions. We are grateful to P. Müller, K. Schlenga, and G. Hechtfischer for the encouragement and the initial technical support of this work. The valuable technical assistance of T. Rapp is gratefully acknowledged. This work was supported by the Bavarian government via the FORSUPRA consortium.

[1] R. Kleiner *et al.*, Phys. Rev. Lett. **68**, 2394 (1992).
[2] R. Kleiner and P. Müller, Phys. Rev. B **49**, 1327 (1994).
[3] F. Steinmeyer *et al.*, Europhys. Lett. **25**, 459 (1994).
[4] J. W. Loram *et al.*, Philos. Mag. B **65**, 1405 (1992).
[5] A. A. Abrikosov, Physica (Amsterdam) **258C**, 53 (1996).
[6] D. C. Ling *et al.*, Phys. Rev. Lett. **75**, 2011 (1995).
[7] I. Taguchi and H. Yoshioka, J. Phys. Soc. Jpn. **29**, 371 (1970).
[8] P. Berberich *et al.*, Physica (Amsterdam) **219C**, 497 (1994); H. Kinder *et al.*, IEEE Trans. Appl. Supercond. **5**, 1575 (1995).
[9] A. Fuchs, W. Prusseit, P. Berberich, and H. Kinder, Phys. Rev. B **53**, 14 745 (1996).
[10] The TBCCO (2223) film was kindly supplied by the IPHT Jena.
[11] V. Ambegaokar and A. Baratoff, Phys. Rev. Lett. **11**, 104 (1963).
[12] B. Mühlschlegel, Z. Phys. **155**, 313 (1959).